Phenomenology of a semi-Dirac semi-Weyl semimetal

S. Banerjee and W. E. Pickett

Phys. Rev. B **86**, 075124 — Published 15 August 2012

DOI: 10.1103/PhysRevB.86.075124

Phenomenology of a semi-Dirac semi-Weyl semi-metal

S. Banerjee[1] and W. E. Pickett[1]
[1]*Department of Physics, University of California, Davis, CA 95616*
(Dated: July 26, 2012)

We extend the semiclassical study of fermionic particle-hole symmetric semi-Dirac (more appropriately, semi-Dirac semi-Weyl) dispersion of quasiparticles, $\varepsilon_K = \pm\sqrt{(k_x^2/2m)^2 + (vk_y)^2)} = \pm\varepsilon_0\sqrt{K_x^4 + K_y^2}$ in dimensionless units, discovered computationally in oxide heterostructures by Pardo and collaborators. This unique system is a highly anisotropic sister phase of both (symmetric) graphene and what has become known as a Weyl semimetal, having $< v_y^2 >^{1/2} \approx v$ independent of energy, and $< v_x^2 >^{1/2} \propto m^{-1/2}\sqrt{\varepsilon}$ being very strongly dependent on energy (ε) and depending only on the effective mass m. Each of these systems is distinguished by bands crossing (sometimes referred to as touching) at a point Fermi surface, with one consequence being that for this semi-Dirac system the ratio $|\chi_{orb}/\chi_{sp}|$ of orbital to spin susceptibilities diverges at low doping. We extend the study of the low-energy behavior of the semi-Dirac system, finding the plasmon frequency to be highly anisotropic while the Hall coefficient scales with carrier density in the usual manner. The Faraday rotation behavior is also reported. For Klein tunneling at normal incidence on an arbitrarily oriented barrier, the kinetic energy mixes both linear (massless) and quadratic (massive) contributions depending on orientation. Analogous to graphene, perfect transmission occurs under resonant conditions, except for the specific orientation that eliminates massless dispersion. Comparisons of the semi-Dirac system are made throughout with both other types of point Fermi surface systems.

PACS numbers:

I. INTRODUCTION

The isolation of single layers of graphite (graphene) with its unique linear (massless Dirac, properly called Weyl) low energy band structure has become, within only a few years, a heavily studied phenomenon.[1,2] The appearance of unanticipated new features in band structures, which generally has far-reaching implications, have in the past included half metallic ferromagnets and compensated half metals ("half metallic antiferromagnets"), and more recently topological insulators.[3,4] Each of these systems provide the promise of not only new physical phenomena but also new applications of their unconventional properties.

Another key feature of graphene is the point Fermi surface aspect. The touching (or crossing) of bands is accompanied by a gap throughout the rest of the Brillouin zone that pins the Fermi level (E_F) in the intrinsic material to lie precisely at the point of crossing – the point Fermi surface (two of them in graphene). This point Fermi surface aspect has been well studied[5] in conventional zero gap semiconductors where a touching of the valence band maximum and conduction band minimum is symmetry determined and occurs at a high symmetry point. The dielectric susceptibility of such a system is anomalous[6] – neither metallic nor semiconducting in character – and unusual consequences of the touching bands and residual Coulomb interaction promise unusual phases, such as excitonic condensates including excitonic superconductors and excitonic insulators.

The linear dispersion at the zone boundary in graphene has been known for many decades; it took the ability to prepare the delicate material and perform a variety of experiments to ignite interest. There are quasilinear (and potentially truly linear) band structure features in certain materials, viz. skutterudites,[7] that have been known for some time and with recent developments[8] may attract new attention. To actually discover a feature in a band structure that provides the quasiparticle dispersion of a new and unexpected type is rare, and the discovery of a semi-Dirac dispersion pinned to the Fermi energy is a very recent example.

Pardo and one of the authors[9,10] reported such a finding in ultrathin (001) VO_2 layers embedded in TiO_2. This new point Fermi surface system, dubbed 'semi-Dirac,' is a hybrid of conventional and unconventional: dispersion is linear ("massless", Dirac-Weyl) in one of the directions of the two-dimensional (2D) layer, and is conventional quadratic ("massive") in the perpendicular direction. At directions between the axes the dispersion is intermediate and highly direction-dependent. Interest in this unique, maximally anisotropic, dispersion arises for several reasons. The (topologically determined pinning at the) point Fermi surface is itself of interest. The highly anisotropic dispersion (from massive to massless depending on angle) is unique to this system. The fact that it arises in an oxide nanostructure of the general type that is grown and studied regularly these days also strengthens the promise of applications. Another layered superstructure, a double cell layer of Ti_3SiC_2 embedded in SiC, has displayed a point Fermi surface, but the dispersion is of the convention type.[11] As alluded to above, an unusual point Fermi surface at zero momentum, with linear bands degenerate with quadratic bands, has been discovered in the skutterudite class of semimetals.[8]

Such a spectrum had been noted earlier in different contexts. Volovik obtained such a spectrum at the point node in the A-phase of superfluid ^{3}He [12] and studied

its topological robustness.[13] More relevant to solids was the discovery by Montambaux's group of this spectrum in a graphene-like model.[14] The model has a broken symmetry such that hopping to two nearest neighbors is t but to the third neighbor is t'. When t' differs from t, the graphene "Dirac points" wander away from the K and K' points, and at $t' = 2t$ they merge, resulting in the semi-Dirac spectrum. This group began a study of low energy properties of such a system,[15] which was continued by Banerjee *et al.*[16] and will be extended in the present paper.

In this paper we first provide results for the Hall coefficient and plasma frequency versus doping level, finding some new behavior along with some somewhat conventional results. Our transport results are obtained within a semiclassical picture, following most transport studies in solids. Further work will be required to address behavior at very low doping level, where a fully quantum treatment is expected to be required. In the final section we provide selected results for Klein tunneling of semi-Dirac particles, a problem that acquires extra richness due to the variable angle of the barrier with respect to the anisotropic dispersion.

II. SEMI-DIRAC DISPERSION

SemiDirac dispersion is quadratic along one symmetry direction in the Brillouin zone and linear along the direction perpendicular to it: massless Dirac(i.e. Weyl). Choosing k_x and k_y to be the momentum variables and taking $\hbar$=1 except occasionally for clarity, the semi-Dirac dispersion is given by:

$$\varepsilon_{\mathbf{k}} = \pm\sqrt{\left[\frac{k_x^2}{2m}\right]^2 + \left[vk_y\right]^2} \tag{1}$$

where the effective mass m applies along k_x and v is the velocity along k_y(the massless direction). For intermediate angles $\beta = \arctan(k_y/k_y)$, the dispersion is of an entirely new type. Two natural scales are introduced, one for the momentum and the other for the energy: $p = 2mv$ (momentum scale) and $\varepsilon_0 = \frac{p^2}{2m} = 2pv$. (Untidy factors of 2 appear because of the clash between the natural classical $\frac{1}{2}pv$ and relativistic pv units for energy.) One can then define the dimensionless momenta $K_X = \frac{\hbar k_x}{p}$ and $K_y = \frac{\hbar k_y}{p}$ in terms of which the semi-Dirac dispersion given by Eq. 1 becomes

$$\varepsilon_{\mathbf{k}} = \pm\varepsilon_0\sqrt{K_x^4 + K_y^2}. \tag{2}$$

The corresponding velocity $\vec{v}_k = \nabla_k\varepsilon_k$ can be scaled to a dimensionless form $\vec{V}_K$ using

$$\vec{V}_K \equiv \frac{\vec{v}_k}{v} = \nabla_K\xi_K \tag{3}$$

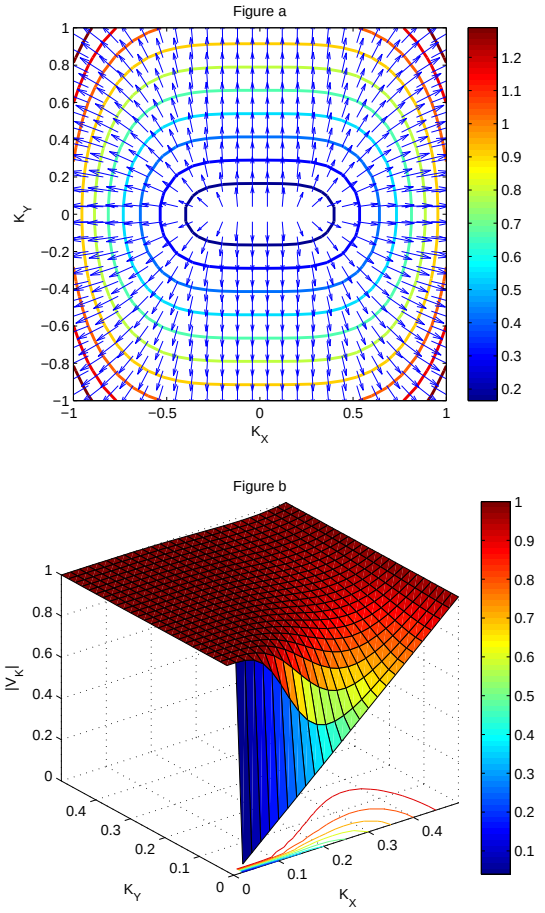

FIG. 1: Fig. a: Fermi-surfaces of semi-Dirac dispersion, along with arrows representing $\vec{V}_{\mathbf{K}}$. The length of an arrow is proportional to the magnitude of $\vec{V}_{\mathbf{K}}$. As can be seen from the figure, the arrow-length is constant along the K_y axis indicating a constant velocity in the relativistic (y) direction. $\vec{V}_{\mathbf{K}}$s are all normal to the constant Fermi energy contours, as they should be. Fig. b: The surface and contour plot of the magnitude of $\vec{V}_{\mathbf{K}}$. The magnitude is constant in the y direction as opposed to the monotonically changing values in the non-relativistic (x) direction, with rapid variation of other directions of propagation.

Figure 1 shows semi-Dirac Fermi surfaces as well as contour plots of $\vec{V}_K$.

We first compute $\langle v_x^2\rangle$ and $\langle v_y^2\rangle$, which are the averages of the Fermi surface velocity $v_F = (\langle v_x^2\rangle + \langle v_y^2\rangle)^{\frac{1}{2}}$ for the semi-Dirac dispersion in the non-relativistic and the relativistic directions respectively, which will prove to be useful later, and will also give the semiclassical conductivity tensor $\sigma_{\alpha\beta} = e^2\tau D(\varepsilon)\langle v_\alpha v_\beta\rangle$. They are defined as follows

$$\begin{aligned}\langle v_\alpha v_\beta(\varepsilon)\rangle &= \sum_k v_\alpha v_\beta\delta(\varepsilon_k - \varepsilon)/\sum_k \delta(\varepsilon_k - \varepsilon) \\ &= \frac{1}{2\pi^2 D(\varepsilon)}\int dk_t \frac{v_\alpha v_\beta}{|v_k|},\end{aligned} \tag{4}$$

where $D(\varepsilon)$ is the density of states. For semi-Dirac dispersion the density of states was obtained earlier[16] as

$$D(\varepsilon) = I_1 \frac{\sqrt{2m\varepsilon}}{\pi^2 v} = I_1 \frac{2m}{\pi^2}\sqrt{\frac{\varepsilon}{\varepsilon_0}}, \tag{5}$$

with proportionality coefficient $\sqrt{m/v^2}$. The integral I_1 is given by

$$I_1 = \int_0^1 ds(1-s^4)^{-\frac{1}{2}} \approx 1.3110. \tag{6}$$

Bácsi *et al.* have studied the quantum critical exponents of point Fermi surface semimetals[17] with $D(\varepsilon) \propto |\varepsilon|^r$ for a continuous range of r including this $r = 1/2$ case.

The squared Fermi velocities for semiDirac dispersion are obtained as

$$\langle v_x^2 \rangle = \frac{4I_3}{I_1}\frac{\varepsilon}{m}, \tag{7a}$$

$$\langle v_y^2 \rangle = \frac{I_2}{I_1}\frac{\varepsilon_0}{m} \approx 1.3v^2, \tag{7b}$$

note that the former involves only m, the latter only v. The integrals I_2 and I_3 are given by

$$I_2 = \int_0^1 ds(1-s^4)^{\frac{1}{2}} \approx 0.8740, \tag{8a}$$

$$I_3 = \int_0^1 ds\frac{s^6}{(1-s^4)^{\frac{1}{2}}} \approx 0.3595, \tag{8b}$$

Thus the ratio of $\langle v_x^2 \rangle$ to $\langle v_y^2 \rangle$ scales as $\varepsilon/\varepsilon_0$, which reflects the extreme anisotropy at small doping. For the VO_2 system where semi-Dirac dispersion was discovered,[9,10] only very small doping levels will remain within the energy range represented by the semi-Dirac dispersion ($\frac{\varepsilon}{\varepsilon_0} \sim 10^{-4}$) but we consider more general cases.

III. FARADAY ROTATION IN THE CONTEXT OF THE SEMI-DIRAC SYSTEM

A. The semiclassical equation of motion

The behavior of point Fermi surface semimetals in a magnetic field has stimulated lively interest due to unusual quantum Hall effect behavior, with the case of graphene having been reviewed recently by Goerbig.[18] The semiclassical equation of motion of an electron in a magnetic field $\vec{B}$ is given by

$$\hbar\frac{d\vec{k}}{dt} = -\frac{e}{c}\vec{v_k} \times \vec{B}. \tag{9}$$

Using Eq. (3) for $\vec{v_k}$ in Eq. (9), one obtains the following expressions

$$\frac{dK_x}{dt} = -\omega_0 K_y, \tag{10a}$$

$$\frac{dK_y}{dt} = 2\omega_0 K_x^3, \tag{10b}$$

where K_x and K_y are the dimensionless variables associated with momentum introduced before, and ω_0 is given by

$$\omega_0 = \frac{eBv^2}{c\varepsilon} = \frac{eB}{mc}\frac{\varepsilon_0}{\varepsilon}, \tag{11}$$

where B is the magnetic field, and ε, the Fermi energy. The Fermi surface orbiting frequency *diverges* as the doping level decreases; the Fermi surface orbit length goes smoothly to zero whereas the mean velocity remains finite. Eliminating K_y from Eqs. (10a) and (10b), the following differential equation is obtained

$$\frac{d^2K_x}{dt^2} = -2\omega_0^2 K_x^3, \tag{12}$$

In order to solve this second order differential equation, we multiply both sides of the equation by $\dot{K_x}$ ($\dot{K_x}$ denotes the time derivative of K_x). Both the right and the left sides of the equation can then be written as a total derivatives, which can be integrated to give

$$\dot{K_x}^2 = -\omega_0^2 K_x^4 + C, \tag{13}$$

where the constant C can be determined from the condition that $\dot{K_x} = 0$ when $K_x = K_{x,\max}$. $K_{x,\max} = (\varepsilon/\varepsilon_0)^{1/2}$ corresponds to $K_y = 0$, from the semiDirac dispersion given by Eq. 2, and the rest follows from Eq. (10a). Hence Eq. 13 becomes

$$\dot{K_x} = \pm\omega_0\sqrt{K_{x,\max}^4 - K_x^4}. \tag{14}$$

Integrating the above equation (numerically) one can get K_x as a function of time. Once K_x is known, K_y can be obtained from Eq. 10b. The differential equation for the cyclotron orbit is obtained by dividing Eq. 10b by Eq. 10a. Solving for that, we obtain the semi-Dirac constant energy contour as an expression for the cyclotron orbit, which is expected, since the energy of an electron does not change when it moves under the influence of magnetic field.

B. The cyclotron frequency

Eq. 14 can be integrated using the limit $-K_{x,\max}$ to $K_{x,\max}$ for the variable K_x to obtain the time period. The result for the time period (T) thus obtained is

$$\omega_0 T = \frac{4I_1}{K_{x,\max}} = 4I_1\sqrt{\varepsilon/\varepsilon_0}, \tag{15}$$

where I_1 is given by Eq. 6. From Eq. 15, the fundamental semi-Dirac cyclotron frequency $\Omega_c \equiv \frac{2\pi}{T}$ is obtained as

$$\Omega_c/\omega_0 = \frac{\pi}{2}I_1^{-1}\sqrt{\varepsilon_0\varepsilon}. \tag{16}$$

The cyclotron frequencies for the parabolic and the linear dispersion cases are given by ($\frac{\mu_B B}{\hbar} = \frac{eB}{mc}$) and $\frac{eBv^2}{c\varepsilon}$ respectively(μ_B is the Bohr magneton). Comparing with Eq. 16 we see that the cyclotron frequencies for all the three cases(the parabolic, linear, and semi-Dirac) depend linearly on the magnetic field. The cyclotron frequency is independent of the Fermi energy for parabolic dispersion, whereas it varies as $\varepsilon^{-\frac{1}{2}}$ for the semiDirac dispersion and as ε^{-1} for the linear Dirac dispersion. One important aspect of the semi-Dirac dispersion is that the semi-Dirac dispersion being anisotropic in the momentum space can have harmonics of the fundamental cyclotron frequency given by Eq. 16. This feature is absent in the Dirac or the two dimensional parabolic dispersion where the energy momentum dispersion is isotropic giving rise to only one value for the cyclotron frequency.

C. Faraday Rotation

The Faraday rotation angle is given by the expression[19]

$$\theta(\omega, B) \;=\; Z_0 f_s(\omega) Re[\sigma_{xy}(\omega, B)], \tag{17}$$

where Z_0 is the impedance of the vacuum, f_s is the spectrally featureless function specific to the substrate, and σ_{xy} is the dynamic Hall conductivity. According to the Drude formula the dynamic Hall conductivity is given by[19]

$$\sigma_{xy} = \frac{-2\mathcal{D}}{\pi} \frac{\omega_c}{\omega_c^2 - (\omega + \frac{i}{\tau})^2}, \tag{18}$$

where $\mathcal{D}$ is the Drude weight, given by $\mathcal{D} = \frac{\pi}{6} e^2 D(\varepsilon) \langle v^2 \rangle$. Taking the real part of Eq. 18 and using it in Eq. 17 we obtain

$$\theta(\omega, B) \;=\; \frac{-2 Z_0 f_s(\omega) \mathcal{D} \omega_c}{\pi} I(\omega), \tag{19}$$

where $I(\omega)$ is given by

$$I(\omega) = \frac{\omega_c^2 - \omega^2 + \frac{1}{\tau^2}}{(\omega_c^2 - \omega^2 + \frac{1}{\tau^2})^2 + \frac{4\omega^2}{\tau^2}} \tag{20}$$

Extremizing $I(\omega)$ and inserting the resulting expression for $I(\omega)$ in Eq. 19 we obtain the following expression for the maximum value of the Faraday rotation angle θ

$$\theta(\omega, B) \;=\; \frac{-Z_0 f_s(\omega) \mathcal{D} \omega_c \tau^2}{2\pi((\omega_c^2 \tau^2 + 1)^{\frac{1}{2}} - 2)}, \tag{21}$$

The Drude weight $\mathcal{D} \sim \varepsilon$ for Dirac dispersion(since $D(\varepsilon) \sim \varepsilon$, and $\langle v^2 \rangle$ is a constant). The Dirac cyclotron frequency $\omega_c \sim \varepsilon^{-1}$. Hence the product $\mathcal{D}\omega_c$ that appears in the numerator of Eq. 21 is independent of the doping level for Dirac dispersion. For semi-Dirac dispersion, $\mathcal{D} \sim \varepsilon^{\frac{1}{2}}$, which follows from the fact that the product $D(\varepsilon)\langle v^2 \rangle \sim D(\varepsilon)\langle v_y^2 \rangle$, where v_y is the speed in the relativistic direction, and that $D(\varepsilon)\langle v_y^2 \rangle \sim \varepsilon^{\frac{1}{2}}$. The last step follows by combining Eq. 5 and Eq. 7b. For the same dispersion $\omega_c \sim \varepsilon^{-\frac{1}{2}}$ (From Eq. 16). Hence, like Dirac dispersion, $\mathcal{D}\omega_c$ for the semi-Dirac dispersion is independent of the doping energy. For two dimensional parabolic dispersion, ω_c is independent of the doping energy, but $\mathcal{D} \sim \varepsilon$. Hence $\mathcal{D}\omega_c$ depends on the doping energy. This is a significant difference when compared to the Dirac and the semi-Dirac dispersion.

For Dirac and semi-Dirac systems the dependence of the Faraday angle on the doping level arises from the term $\omega_c \tau$ in the denominator of Eq. 21, whereas the numerator is independent of doping. For those dispersions one can fine tune the Fermi energy to obtain a large value of the Faraday angle by bringing the term $\omega_c \tau$ close to three, so that the term $(\omega_c^2 \tau^2 + 1)^{\frac{1}{2}} - 2$ appearing in denominator goes to zero causing a significant value for the Faraday angle.

IV. HALL COEFFICIENT

According to semiclassical Bloch-Boltzmann transport theory, the Hall coefficient of a two dimensional Fermi liquid (in the $x-y$ plane) is[20]

$$R^H \equiv R^H_{xyz} = \frac{\Sigma_{\mathbf{k}} v_x(\mathbf{k}) [\mathbf{v}(\mathbf{k}) \times \nabla(\mathbf{k})]_z v_y(\mathbf{k}) (\frac{-\partial f}{\partial \varepsilon})}{[\Sigma_{\mathbf{k}} v_x^2(\mathbf{k}) (\frac{-\partial f}{\partial \varepsilon})][\Sigma_{\mathbf{k}} v_y^2(\mathbf{k}) (\frac{-\partial f}{\partial \varepsilon})]}. \tag{22}$$

Due to the algebraic complexity of the first and second derivatives of ξ_K, this expression is formally unwieldy. We show however that general properties of this expression lead to a simple and familiar result for R_H.

The numerator of Eq. (22) is the area A_v spanned by the velocity vector over the Fermi surface[21]. In the zero temperature limit each term in the denominator reduces to a line integral along the Fermi-surface. The carrier density n is proportional to the area swept by the vector $\mathbf{k}$ over the Fermi surface, which is the area A_{FS} enclosed by the Fermi surface. Hence the quantity $R^H n$ is given by:

$$R^H n = \frac{A_v A_{FS}}{\oint dk_l \frac{v_x^2}{v_k} \oint dk_l \frac{v_y^2}{v_k}}. \tag{23}$$

Using the fact that the gradient $\nabla_{\mathbf{k}} \varepsilon$ is perpendicular to the vector line element $d\mathbf{k}_l$ along the Fermi surface, so that the dot product between them is zero, the denominator of Eq. (23) reduces to

$$\oint dk_l \frac{v_x^2}{v_k} \oint dk_l \frac{v_y^2}{v_k} = \oint dk_y v_x \oint dk_x v_y. \tag{24}$$

Using Eq. (24) in Eq. (23) we obtain

$$R^H n = \frac{A_v A_{FS}}{\oint dk_y v_x \oint dk_x v_y}. \tag{25}$$

$R^H n$ as given by Eq. (25) is unity for the semi-Dirac dispersion. This result can be argued directly from equation Eq. (25) in the following way. The semi-Dirac dispersion is symmetric both in the x and the y directions. Hence we can restrict the limits of the integrals appearing in Eq. (25) to the first quadrant. For the first term in the denominator of Eq. (25), carrying out the integration by parts one obtains:

$$-\int dk_y v_x = -k_y v_x|_i^f + \int dv_x k_y \tag{26}$$

i and f correspond to the points on the Fermi surface with $k_y = 0$ and $k_x = 0$ respectively. The boundary terms in Eq. (26) at i and f are zero because k_y and the x component of the gradient at the semi-Dirac Fermi surface vanish at i and f respectively. Using the above reasoning the first term in the denominator of Eq. (25) is changed to $\int dv_x k_y$. Making use of this along with the definition of area under a curve(for the terms in the numerator), Eq. (25) can be written as

$$R^H n = -\frac{\int dk_x k_y \int dv_x v_y}{\int dv_x k_y \int dk_x v_y}. \tag{27}$$

v_y for the semiDirac dispersion evaluated on the Fermi surface turns out to be proportional to k_y as can be seen from Eq. (2). Hence it is observed that in Eq. (27) the numerator and the denominator are equal except for a minus sign. That explains why we obtain $R^H n = -1$ for the semiDirac dispersion. Incidentally, v_y is proportional to k_y for the Dirac and the parabolic dispersion relations. Hence, $R^H n$ is equal to -1 for those dispersions too. So it can be said that the Hall coefficient times the carrier density is a topologically invariant quantity for a certain class of band structures, reminiscent of the geometrical representation of Ong.[21]

V. PLASMON FREQUENCY

The plasmon frequency for the semiDirac system can be computed by setting the random phase approximation expression for the dielectric constant

$$\epsilon(\mathbf{q},\omega) = 1 - v(\mathbf{q})\chi_0(\mathbf{q},\omega) \tag{28}$$

to zero.[22,23] $\chi_0(\mathbf{q},\omega)$ is the polarizability and $v(\mathbf{q})$ is the Fourier transform of the Coulomb potential. $\chi_0(\mathbf{q},\omega)$ is given by the Lindhard expression

$$\chi_0(\mathbf{q},\omega) = \int \frac{d^2k}{(2\pi)^2} \frac{f(\varepsilon_{\mathbf{k}}) - f(\varepsilon_{\mathbf{k+q}})}{\omega + \varepsilon_{\mathbf{k}} - \varepsilon_{\mathbf{k+q}}}. \tag{29}$$

Expanding $\varepsilon_{\mathbf{k+q}}$ in Eq. 29 for small $\mathbf{q}$ (we treat only this regime), the numerator in Eq. 29 takes the following form at low temperature

$$f(\varepsilon_{\mathbf{k}}) - f(\varepsilon_{\mathbf{k+q}}) = \vec{v}_k \cdot \vec{q}\delta(\varepsilon_{\mathbf{k}} - \varepsilon). \tag{30}$$

Expanding the denominator as well, Eq. 29 becomes

$$\chi_0(\mathbf{q},\omega) = \int \frac{d^2k}{(2\pi)^2} \frac{\vec{v}_k \cdot \vec{q}}{\omega}(1 + \frac{\vec{v}_k \cdot \vec{q}}{\omega})\delta(\varepsilon_{\mathbf{k}} - \varepsilon). \tag{31}$$

The Coulomb potential $v(\mathbf{q})$ in two dimensions is

$$v(\mathbf{q}) = \frac{2\pi e^2}{\kappa q}, \tag{32}$$

where $q = \sqrt{q_x^2 + q_y^2}$, and κ is the background dielectric constant of the medium. Using Eq. 31 and Eq. 32 in Eq. 28, and setting $\epsilon(q,\omega) = 0$, the plasmon frequency is

$${\omega_p}^2 = \frac{8I_3}{\pi}\frac{e^2 q\varepsilon_0}{\kappa}F(\theta), \tag{33}$$

where $F(\theta)$ is given by

$$F(\theta) = \xi^{\frac{3}{2}}(\cos^2\theta + \frac{1}{4}\xi^{-1}\frac{I_2}{I_3}\sin^2\theta), \tag{34}$$

and I_2, I_3 are given by Eq. 8a and in Eq. 8b respectively. ε_0 is the energy scale defined earlier. θ denotes the angle that the plasmon wave-vector makes with the non-relativistic axis k_x of the semi-Dirac dispersion. Recall that the Fermi energy variable is defined as $\xi \equiv \frac{\varepsilon}{\varepsilon_0}$. $\omega_p \propto \sqrt{q}$ is characteristic of a two-dimensional system.

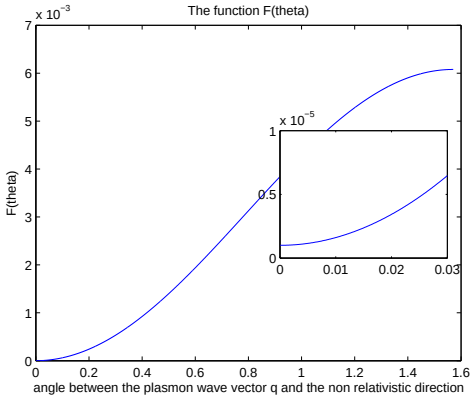

FIG. 2: Angular dependence of the function F

The function $F(\theta)$ is plotted against θ in Fig. 2. Using Eq. 5 for the semiDirac density of states and Eq. 7a and Eq. 7b for the mean square Fermi velocities, Eq. 33 reduces to

$${\omega_p}^2 = \pi\frac{e^2 q\hbar D(\varepsilon)}{\kappa}(\langle v_x^2\rangle\cos^2\theta + \langle v_y^2\rangle\sin^2\theta). \tag{35}$$

The plasmon frequency is highly anisotropic and reaches its maximum along the relativistic direction, which could be a signature characteristic of s semiDirac system.

VI. MAGNETIC SUSCEPTIBILITY

In this section we consider the magnetic susceptibilities for the semi-Dirac dispersion. The Pauli spin susceptibility is given by

$$\chi_{sp}/\mu_B^2 = D(\varepsilon), \tag{36}$$

where $D(\varepsilon)$ is the density of states. Using Eq. 5 for the semi-Dirac density of states Eq. 36 reduces to

$$\chi_{sp}/\mu_B^2 = \frac{2m}{\pi^2}\sqrt{\xi}, \tag{37}$$

where ξ is the same dimensionless variable related to the Fermi energy appearing in the previous section. For a non-interacting Fermi liquid the orbital susceptibility is given by[24]

$$\begin{aligned}\chi_{orb}/\mu_B^2 &= -\frac{m^2}{12\pi^3}\int d^2\mathbf{k}[\frac{\partial^2\varepsilon_{\mathbf{k}}}{\partial k_x^2}\frac{\partial^2\varepsilon_{\mathbf{k}}}{\partial k_y^2}+2(\frac{\partial^2\varepsilon_{\mathbf{k}}}{\partial k_x\partial k_y})^2 \\ &+\frac{3}{2}(\frac{\partial\varepsilon_{\mathbf{k}}}{\partial k_x}\frac{\partial^3\varepsilon_{\mathbf{k}}}{\partial k_x\partial k_y^2}+\frac{\partial\varepsilon_{\mathbf{k}}}{\partial k_y}\frac{\partial^3\varepsilon_{\mathbf{k}}}{\partial k_y\partial k_x^2})]\delta(\varepsilon-\varepsilon_{\mathbf{k}})\end{aligned} \tag{38}$$

Using Eq. 2 for $\varepsilon_{\mathbf{k}}$ in Eq. 38 and doing the integral we obtain

$$\chi_{orb}/\mu_B^2 = -\frac{2\sqrt{2}I_4}{3\pi^3}\frac{m^{\frac{3}{2}}v}{\varepsilon^{\frac{1}{2}}}, \tag{39}$$

where the integral I_4 is given by

$$I_4 = \int_0^1 d\alpha\frac{-33\alpha^{10}+41\alpha^6-9\alpha^2}{(1-\alpha^4)^{\frac{1}{2}}}. \tag{40}$$

Evaluating the numerical value for I_4 and using the dimensionless variable ξ, Eq. 39 reduces to

$$\chi_{orb}/\mu_B^2 = -\frac{0.0798m}{\pi^3}\sqrt{\frac{\varepsilon_0}{\varepsilon}}. \tag{41}$$

We observe that the orbital susceptibility for the semi-Dirac system is always diamagnetic. The absolute value of the ratio of the spin to the orbital susceptibilities (the ratio of Eq. 37 to Eq. (41)) of the semi-Dirac dispersion is given by

$$|\frac{\chi_{sp}}{\chi_{orb}}| \sim 80m\xi \tag{42}$$

Hence orbital magnetic susceptibility for the semi-Dirac dispersion dominates the spin susceptibility at low energy. This result is distinct qualitatively from both the Dirac and the parabolic dispersion cases. For the doped Dirac dispersion the orbital susceptibility vanishes identically. For conventional two dimensional parabolic dispersion the orbital susceptibility calculated using Eq. 38is found to be 6π times smaller than its spin susceptibility. Hence the unusually large orbital susceptibility can be considered a distinctive feature of the semi-Dirac dispersion.

VII. HEAT CAPACITY

We show here how the heat capacity for the non-interacting *two*-dimensional semi-Dirac electron gas is similar to that of the *three*-dimensional non-interacting electron gas with the parabolic energy-momentum dispersion at both the low and the high temperature ends. The similarity becomes equality at high temperature. Relative to the natural energy scale ε_0 introduced at the beginning, the low and the high temperatures can be considered. The low temperature heat capacity per particle for the semiDirac dispersion is :

$$c_v = \frac{2I_1}{3}mk_B^2T\sqrt{\frac{\varepsilon}{\varepsilon_0}}, \tag{43}$$

which is calculated using Sommerfeld expansion[25](I_1 is given in Eq. 6). It is observed that the heat capacity in Eq. 43 is proportional to $D(\varepsilon)\propto\sqrt{\varepsilon}$, as it must be because c_v depends only on the spectrum of energy levels. A similar type of dependence with energy is observed for the three dimensional electron gas with the parabolic energy-momentum dispersion. The difference between them is in the prefactors. This difference disappears quite nicely in the high temperature end as is shown in the following. At high temperature, the heat capacity for the three dimensional electron gas is given by $\frac{3}{2}k_B$. In order to emphasize a technique that will be used for the semi-Dirac problem, a derivation of the above result for the three-dimensional electron gas is first outlined in the following. The parabolic three dimensional Hamiltonian is given by $H_{\text{parabolic}} = \frac{1}{2m}(p_x^2+p_y^2+p_z^2)$, so it follows that $\frac{\partial H_{\text{parabolic}}}{\partial p_i} = \frac{p_i}{m}$ [where $i = x, y, z$]. Hence $H_{\text{parabolic}}$ can be written as

$$\begin{aligned}H_{\text{parabolic}} &= \frac{1}{2}(p_x\frac{\partial H_{\text{parabolic}}}{\partial p_x} \\ &+p_y\frac{\partial H_{\text{parabolic}}}{\partial p_y}+p_z\frac{\partial H_{\text{parabolic}}}{\partial p_z}).\end{aligned} \tag{44}$$

By the equipartition theorem, the ensemble average of each of $p_x\frac{\partial H_{\text{parabolic}}}{\partial p_x}, p_y\frac{\partial H_{\text{parabolic}}}{\partial p_y}$, and $p_z\frac{\partial H_{\text{parabolic}}}{\partial p_z}$ is k_BT.[26] Hence taking the ensemble average of the Hamiltonian in Eq. 44, one obtains

$$< H_{\text{parabolic}} >= \frac{3}{2}k_BT. \tag{45}$$

The derivative of $< H_{\text{parabolic}} >$ with respect to T gives the heat capacity as $\frac{3}{2}k_B$.

Next, the classical semi-Dirac Hamiltonian is given by

$$H_{\text{sD}} = \sqrt{\frac{p_x^4}{4m^2}+v^2p_y^2} \tag{46}$$

Taking the derivatives of H_{sD} with respect to p_x and p_y gives, in spite of its complex form, the analogous expression

$$H_{\text{sD}} = \frac{1}{2}p_x\frac{\partial H_{\text{sD}}}{\partial p_x}+p_y\frac{\partial H_{\text{sD}}}{\partial p_y} \tag{47}$$

In the same way as before, by the equipartition theorem, the averages of each of $p_x \frac{\partial H_{\rm sD}}{\partial p_x}, p_y \frac{\partial H_{\rm sD}}{\partial p_y}$ is $k_B T$. Hence the ensemble average of $H_{\rm sD}$ is given by

$$< H_{\rm sD} >= \frac{1}{2} k_B T + k_B T = \frac{3}{2} k_B T \tag{48}$$

thus $c_v = \frac{3}{2} k_B$ for semi-Dirac dispersion in the high T limit. This result is exactly that of a three dimensional non-interacting gas with parabolic dispersion.

This rather unexpected result can also be obtained directly starting from the Boltzmann distribution. In the low temperature limit the semi-Dirac heat capacity has the same T dependence as the non-interacting three dimensional parabolic system. In the high temperature end of the spectrum the heat capacities are identical. Hence a two dimensional semi-Dirac system effectively behaves as a three dimensional system so far as heat capacities are concerned. The appearance of this third degree of freedom can have potential technological applications. For example, a semi-Dirac nanostructure could be used as an efficient heat sink. More generally, a semi-Dirac system can function quite differently compared to other two dimensional systems for thermal management as well as for many other applications.

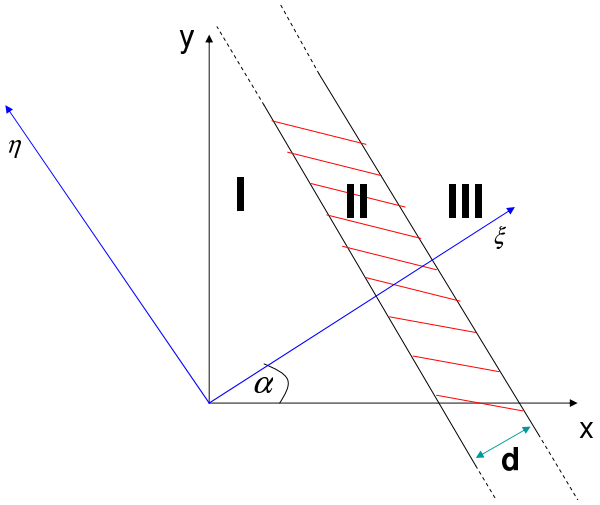

FIG. 3: The top view of the potential barrier is shown. It extends infinitely in one direction ($\hat{\eta}$ direction), but limited to a spatial length d in the orthogonal direction ($\hat{\xi}$ direction), which makes an angle α with the non-relativistic direction. An electron with energy E is incident normally on the potential, i.e, along the $\hat{\xi}$ direction.

VIII. KLEIN TUNNELING

The Klein paradox is the name given to the phenomenon of the complete transmission of a particle at selected energies or geometric configurations through a potential barrier even when the barrier is arbitrarily high. For the conventional tunneling problem, the probability of transmission decreases exponentially with the height and thickness of the barrier. In order for Klein tunneling to take place, there must be hole states having negative energies available to promote tunneling. The positive potential in the barrier region raises the hole states, making them available. For 'relativistic' Dirac-Weyl dispersion (as in graphene) Katsnelson and collaborators[27] have shown that Klein tunneling can occur and that transmission is unusually robust at near-normal incidence. Klein tunneling is also possible in conventional (massive) zero-gap semiconductors including double-layer graphene,[27] with an angular behavior that is distinct from that of graphene. Klein tunneling therefore is expected for particles with semiDirac dispersion, but there should be many distinctions. The low-energy Hamiltonian corresponding to the semiDirac dispersion can be taken as[16]

$$H = v \hat{p}_y \tau_3 + \frac{\hat{p}_x^2}{2m} \tau_1, \tag{49}$$

where the τ's are the Pauli matrices in orbital space and $\hat{p}_{x(y)}$ are the momentum operators.

A. Rotation of the Frame

The semi-Dirac system is (highly) anisotropic. The potential barrier can be oriented at an arbitrary angle with respect to the $\hat{x}, \hat{y}$ axes,after which one might consider a particle impinging on the barrier from another arbitrary angle. This extension from the isotropic systems of graphene or zero-gap semiconductors leads to a rather complicated tunneling problem that could form the basis of a separate study. To keep the algebra and the physical picture as simple as possible, we consider only the special case of *normal incidence* of a semi-Dirac quasi-particle onto a potential barrier of width d, which is inclined at an angle $\frac{\pi}{2} + \alpha$ with respect to the x(nonrelativistic) axis as shown in Fig.3. A set of orthogonal axes ξ and η with respect to the barrier are defined. $\hat{\eta}$ is the direction along which the potential is infinitely extended. The electron is incident on the potential along $\hat{\xi}$, which makes an angle α with respect to the $\hat{x}$ axis. The barrier has thickness d along the ξ axis. We work in the regime where the energy of the incident semi-Dirac particle is small compared to the barrier potential. There are three real space regions: to the left of the barrier where the potential is zero; within the barrier with positive potential V; and to the right of the barrier where again the potential vanishes. We refer to these regions as I, II, and III, respectively, and the wavefunctions are denoted by Ψ_I, Ψ_{II}, Ψ_{III}, respectively. The momentum operators along the x and the y (relativistic) directions can be written in terms of

the variables ξ and η as follows:

$$\begin{aligned} \hat{p}_x &= \hat{p}_\xi \cos\alpha - \hat{p}_\eta \sin\alpha \\ \hat{p}_y &= \hat{p}_\xi \sin\alpha + \hat{p}_\eta \cos\alpha, \end{aligned} \tag{50}$$

where $\hat{p}_{\xi(\eta)}$ are the corresponding momentum operators given by $-i\partial/\partial\xi(\eta)$. Since we are considering incidence normal to the barrier, it is straightforward to show that the η degree of freedom can be eliminated from the problem. The Hamiltonian in Eq. 49 takes the following form:

$$\begin{aligned} H &= v\hat{p}_\xi \sin\alpha\tau_3 + \frac{\hat{p}_\xi^2}{2m}\cos^2\alpha\tau_1 \\ &= v_\alpha \hat{p}_\xi \tau_3 + \frac{\hat{p}_\xi^2}{2m_\alpha}\tau_1. \end{aligned} \tag{51}$$

This transformed kinetic "Hamiltonian" has both linear (massless) and quadratic (massive) contributions, governed an increased mass $m_\alpha = m/cos^2\alpha$ and a decreased velocity $v_\alpha = vsin\alpha$. Thus the orientation of the barrier allows the tuning of the relative amounts of linear and quadratic dispersion. In the limits $\alpha = 0$ and $\pi/2$, the problem reverts to the problem for zero-gap semiconductors and for graphene, respectively.

For a value of α between these limits the forward propagating wave, which is of the form $e^{ik\xi}$ times a spinor, is still an admissible eigenstate of the Hamiltonian. Operating on the planewave with the Hamiltonian in Eq. 51 gives an expression that can be written as

$$H_k = vk\sin\alpha[\tau_3 + \tau_1\tan\theta], \tag{52}$$

where

$$\tan\theta = \frac{\cos^2\alpha}{\sin\alpha}\frac{k}{2mv} = \frac{k}{2m_\alpha v_\alpha} = \frac{k}{p_\alpha}. \tag{53}$$

Thus $tan\theta$ reflects the magnitude of the particle momentum relative to the scaled semi-Dirac momentum $p_\alpha = 2m_\alpha v_\alpha$. When $\mathbf{k}$ goes to $-\mathbf{k}$ as is the case when one considers the backward propagating wave $e^{-ik\xi}$, aside from the positive multiplicative factor vk which changes sign, the Hamiltonian in Eq. 51 changes from $\tau_3+\tau_1\tan\theta$ to $-[\tau_3 - \tau_1\tan\theta]$. The corresponding eigensystems are given for quick reference in the Appendix.

B. Derivation of the Resonance Condition

The time independent Schrodinger equation in a given potential can be written as

$$h\psi = (E-V)\psi, \tag{54}$$

where h is the part of the Hamiltonian without the potential V. In regions I and III $(E-V)$ is positive, and the positive eigenvalue form of the solution as given by Eq. A2a in the Appendix for the forward propagating wave and by Eq. A4a for the backward propagating wave need to be considered in those regions. In region II, V being much larger than E results in $(E-V)$ being negative. Hence the negative eigenvalue solutions as given by Eq. A2b and Eq. A4b appearing in the appendix are of importance in that region. Momenta in regions I and III are equal, denoted by k_1, and denoted by k_2 in region II. k_1 and k_2 are given by

$$vk_1\sin\alpha(\cos\theta_1)^{-1} = E, \tag{55a}$$

$$vk_2\sin\alpha(\cos\theta_2)^{-1} = V - E, \tag{55b}$$

where θ_1 and θ_2 are given by

$$\tan\theta_{1(2)} = \frac{\cos^2\alpha}{\sin\alpha}\frac{k_{1(2)}}{2mv} = \frac{k_{1(2)}}{p_\alpha} \tag{56}$$

Finally, the wave functions in the three regions are

$$\begin{aligned} \Psi_I &= e^{ik_1\xi}\begin{pmatrix}\cos(\theta_1/2)\\ \sin(\theta_1/2)\end{pmatrix} \\ &+ re^{-ik_1\xi}\begin{pmatrix}\sin(\theta_1/2)\\ \cos(\theta_1/2)\end{pmatrix}, -\infty < x < 0, \\ \Psi_{II} &= t_1 e^{ik_2\xi}\begin{pmatrix}\sin(\theta_2/2)\\ -\cos(\theta_2/2)\end{pmatrix} \\ &+ r_1 e^{-ik_2\xi}\begin{pmatrix}\cos(\theta_2/2)\\ -\sin(\theta_2/2)\end{pmatrix}, 0 < x < d, \\ \Psi_{III} &= t_2 e^{ik_1\xi}\begin{pmatrix}\cos(\theta_1/2)\\ \sin(\theta_1/2)\end{pmatrix}, d < x < \infty, \end{aligned} \tag{57}$$

where r,t_1,r_1 and t_2 are constants determined by matching. The absolute square of t_2 gives the transmission coefficient. Matching the wave functions at the boundaries $y = 0$ and $y = d$, one obtains for the transmission

$$|t_2|^2 = \frac{(\sin\theta_2\cos\theta_2\cos\theta_1)^2}{A^2 + B^2 - 2AB\cos k_2 d}, \tag{58}$$

where A and B are given by:

$$\begin{aligned} A &= [\sin((\theta_2-\theta_1)/2)\cos\theta_2 \\ &\quad + \sin(\theta_2+\theta_1)/2]\cos((\theta_2-\theta_1)/2) \\ B &= \sin\theta_2\sin^2((\theta_2+\theta_1)/2) \end{aligned} \tag{59}$$

It can be shown that when

$$\cos k_2 d = 1 \tag{60}$$

the denominator in Eq. 58 becomes equal to the numerator. The resonance condition as given by Eq. 60 implies

$$k_2 d = 2n\pi; \rightarrow k_2 = np_d \tag{61}$$

where n is an integer and the characteristic momentum scale $p_d = 2\pi/d$ has been introduced. From Eq. 55b and Eq. 61 we obtain the following condition for complete transmission of an incident wave:

$$[n^2\sin^2\alpha + n^4\cos^4\alpha(\frac{\pi}{mvd})^2]^{\frac{1}{2}} = \frac{(V-E)d}{2\pi v} \tag{62}$$

or equivalently in terms of "renormalized" constants

$$n[1+n^2(\frac{p_d}{p_\alpha})^2]^{\frac{1}{2}} = \frac{(V-E)}{p_d v_\alpha}. \quad (63)$$

Eq. 63 gives the resonance condition, either for resonant energies $E_n(\alpha, d, V)$ or for orientations $\alpha_n(d, V-E)$, for full transmission.

The limiting cases are $\alpha \to 0$ and $\alpha \to \pi/2$. The latter limit corresponds to normal incidence of a particle with 'relativistic' Dirac-Weyl dispersion which is treated in Ref. [27], where it was shown that there is complete transmission even if the potential barrier is large. The resonance condition for this limiting case can be obtained setting $\alpha = \pi/2$ in Eq. 63. The $\alpha = 0$ limit becomes the case of conventional massive particle tunneling, which must be treated separately (see the following subsection). The semi-Dirac system provides for, and interpolates between smoothly, the two very different limits. Figure 4 provides a schematic illustration where there is a single resonant orientation of the barrier.

C. Limiting case $\alpha = 0$

This case corresponds to the potential being perpendicular to x (the non-relativistic direction), so k_y=0. The Hamiltonian admits *evanescent* as well as propagating wave solutions only in this case; in a sense the relativistic character dominates the behavior except at α=0. It is instructive to follow the mixing of the positive and negative energy components. Operating on propagating waves $e^{\pm ik_x x}$ the Hamiltonian in Eq. 49 takes the following form in the **k** space:

$$H = \frac{k_x^2}{2m}\tau_x, \quad (64)$$

with the conventional massive eigenvalues $\pm\frac{k_x^2}{2m}$. For evanescent waves the eigenvalues are interchanged, resulting in a mixing of positive and negative energy functions in a way that does not occur with non-zero k_y.

The energy of the incident particle for both the propagating and the evanescent cases are the same:($E = \frac{k_x^2}{2m}$). The momenta in regions $\{I, III\}$ and II are denoted by $k_1'' = \sqrt{2mE}$ and $k_2'' = \sqrt{2m|V-E|}$ respectively. The form of the wave function in the three regions are

$$\begin{aligned}
\Psi_I &= e^{ik_1'' x}\begin{pmatrix}1\\1\end{pmatrix} + r'' e^{-ik_1'' x}\begin{pmatrix}1\\1\end{pmatrix} \quad (65)\\
&\quad + t''' e^{k_1'' x}\begin{pmatrix}1\\-1\end{pmatrix},\\
&\quad -\infty < x < -d,\\
\Psi_{II} &= t_1'' e^{ik_2'' x}\begin{pmatrix}1\\-1\end{pmatrix} + r_1'' e^{-ik_2'' x}\begin{pmatrix}1\\-1\end{pmatrix}\\
&\quad + t_1''' e^{k_2'' x}\begin{pmatrix}1\\1\end{pmatrix} + r_1''' e^{-k_2'' x}\begin{pmatrix}1\\1\end{pmatrix},\\
&\quad -d < x < d,\\
\Psi_{III} &= t_2'' e^{ik_1'' x}\begin{pmatrix}1\\1\end{pmatrix} + r_2''' e^{-k_1'' x}\begin{pmatrix}1\\-1\end{pmatrix},\\
&\quad d < x < \infty,
\end{aligned}$$

where $r'', t''', t_1'', r_1'', t_1''', r_1''', t_2'', r_2'''$ are constants. In Eq. 65, for regions I and III the evanescent waves are constructed in such a way that they don't diverge when $|x|$ becomes large. There is no backward traveling wave in region III. $|t_2''|^2$ is the transmission coefficient.

Equating the wave function and its derivative at the boundaries $x = 0$ and $x = d$, for the transmission coefficient we obtain

$$|t_2''|^2 = |\frac{4ik_1''k_2'' e^{-ik_2'' d}}{e^{-k_2'' d}(k_2''+ik_1'')^2 - e^{k_2'' d}(k_2''-ik_1'')^2}|^2. \quad (66)$$

Eq. 66 is the same as that given by Katsnelson *et al.*[27] in the context of the tunneling probability for the bilayer graphene dispersion. k_2'' gets large as the potential V gets large. Because of the presence of the exponential factor $e^{k_2'' d}$ in the denominator, the transmission coefficient given by Eq. 66 goes to zero as the potential goes to infinity. Thus there is no perfect transmission when the potential is in the non relativistic direction and the particle is incident normally, as mentioned above.

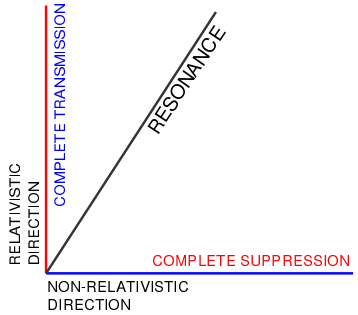

FIG. 4: Complete transmission for various orientations of the potential

IX. SUMMARY

In this paper several low energy properties of the semi-Dirac, semi-Weyl degenerate semimetal have been studied. Whereas some of the properties are intermediate between the conventional parabolic and the linear "Dirac" (graphene) dispersion, as is the case for the cyclotron frequency, some other properties can be distinct and rather unusual. The dependence of the Hall coefficient nevertheless depends on doping level in the usual way, and we illuminate how this result is related to the form of the dispersion relation. Results for Klein tunneling for the case of semi-Dirac dispersion have been obtained for normal incidence on an arbitrarily oriented barrier in the 2D plane, revealing that an electron can tunnel through the barrier with probability one, subject to a resonance condition being met, *except* for the direction where linear dispersion does not enter the problem. The extreme anisotropy of the plasmon frequency is a distinctive feature of a semi-Dirac system.

Intriguing behavior for the Faraday rotation and the low- to high-temperature crossover of the heat capacity have been provided. Finally, we note that the behavior of the orbital susceptibility is distinct from both quadratic and linear systems, being strongly dependent on doping level. Also we remind that our transport results have been obtained within the semiclassical approximation. Several properties of graphene require treatment beyond the semiclassical one[28,29] at very low doping, and we anticipate that the semi-Dirac system may be even more delicate in this limit than is graphene.

X. ACKNOWLEDGMENTS

This project was supported by DOE grant DE-FG02-04ER46111 and was facilitated by interactions within the Predictive Capability for Strongly Correlated Systems team of the Computational Materials Science Network.

Appendix A: 2×2 eigensystems

I. The eigenvalues $\lambda_\pm$ and eigenstates $\Lambda_\pm$ of the 2 by 2 real matrix

$$\tau_z + \tan\theta\tau_x \tag{A1}$$

are given by:

$$\lambda_+ = (\cos\theta)^{-1}; \quad \Lambda_+ = \begin{pmatrix}\cos(\theta/2)\\ \sin(\theta/2)\end{pmatrix}, \tag{A2a}$$

$$\lambda_- = -(\cos\theta)^{-1}; \quad \Lambda_- = \begin{pmatrix}\sin(\theta/2)\\ -\cos(\theta/2)\end{pmatrix}. \tag{A2b}$$

II. For the matrix

$$-[\tau_z - \tan\theta\tau_x], \tag{A3}$$

the eigensystems are

$$\lambda_+ = (\cos\theta)^{-1}: \quad \Lambda_+ = \begin{pmatrix}\sin(\theta/2)\\ \cos(\theta/2)\end{pmatrix}, \tag{A4a}$$

$$\lambda_- = -(\cos\theta)^{-1}: \quad \Lambda_- = \begin{pmatrix}\cos(\theta/2)\\ -\sin(\theta/2)\end{pmatrix}. \tag{A4b}$$

[1] K.S. Novoselov, A.K. Geim, S.V. Morozov, D. Jiang, M.I. Katsnelson, I.V. Grigorieva, S.V. Dubonos, A.A. Firsov, Nature **438**, 197 (2005).

[2] A. H. Castro Neto, F. Guinea, N. M. R. Peres, K. S. Novoselov, A. K. Geim, Rev. Mod. Phys. **81**, 109 (2009).

[3] M. Z. Hasan and C. L. Kane, Rev. Mod. Phys. **82**, 3045 (2010).

[4] X.-L. Qi and S. C. Zhang, Rev. Mod. Phys. **83**, 1057 (2011).

[5] I. M. Tsidilkovski, *Gapless Semiconductors - a New Class of Materials* (Akademie-Verlag Berlin, Berlin, 1988).

[6] D. Sherrington and W. Kohn, Phys. Rev. Lett. **21**, 153 (1968).

[7] D. J. Singh and W. E. Pickett, Phys. Rev. B (RC) **50**, 11235 (1994).

[8] J. C. Smith, S. Banerjee, V. Pardo, and W. E. Pickett, Phys. Rev. Lett. **106**, 056401 (2011).

[9] V. Pardo and W. E. Pickett, Phys. Rev. Lett. **102**, 166803 (2009).

[10] V. Pardo and W. E. Pickett, Phys. Rev. B **81**, 035111 (2010)

[11] Z. Wang, S. Tsukimoto, R. Sun, M. Saito, and Y. Ikuhara, Appl. Phys. Lett. **98**, 104101 (2011).

[12] G. E. Volovik, Pis'ma ZhETF **73**, 182 (2001) [Sov. Phys. JETP **73**, 162 (2001).

[13] G. E. Volovik, *The Universe in a Helium Droplet* (Clarendon Press, Oxford, 2003).

[14] P. Dietl, F. Piéchon, and G. Montambaux, Phys. Rev. Lett. **100**, 236405 (2008).

[15] P. Delplace and G. Montambaux, Physical review B **82**, 035438 (2010)

[16] S. Banerjee, R. R. P. Singh, V. Pardo, and W. E. Pickett, Phys. Rev. Lett. **103**, 016402 (2009).

[17] A. Bácsi, A. Virosztek, L. Borda, and B. Dóra, Phys. Rev. B **82**, 153406 (2010).

[18] M. O. Goerbig, Rev. Mod. Phys. **83**, 1193 (2011).

[19] I. Crassee, J. Levallois, A. L. Walter, M. Ostler, A. Bostwick, E. Rotenberg, T. Seyller, D. van der Marel, A. B.

Kuzmenko, Nature Physics **7**, 48 (2011).
[20] P. B. Allen, W. E. Pickett, and H. Krakauer, Phys. Rev. B **37**, 7482 (1988).
[21] N. P. Ong, Phys. Rev. B **43**, 193 (1991).
[22] S. Das Sarma, E. H. Hwang, Phys. Rev. Lett. **102**, 206412 (2009).
[23] E. H. Hwang and S. Das Sarma, Physical review B **75**, 205418 (2007)
[24] H. Fukuyama, Progress of Theoretical Physics **45**, 3 (1971).
[25] N. W. Ashcroft,N. D. Mermin *Solid State Physics* (Brooks/Cole, 1976), p. 47.
[26] W. Greiner,L. Neise and H. St$\breve{}$cker, *Thermodynamics and Statistical Mechanics* (Springer-Verlag, 1995), p. 196.
[27] M. I. Katsnelson, K. S. Novoselov, A. K. Geim, Nature Physics **2**, 620-625 .
[28] T. Ando, Y. Zheng, H. Suzuura, J. Phys. Soc. Jpn **71**, 1318 (2002).
[29] N. M. R. Peres, F. Guinea, and A. H. Castro Neto, Phys. Rev. B **73**, 125411 (2006).